UCRL-JC-130648
PREPRINT

High Accuracy Capture of Curved Shock Fronts Using the Method of Space-Time Conservation Element and Solution Element

Grant Cook, Jr.

This paper was prepared for submittal to the
37th AIAA (American Institute of Aeronautics and Astronautics)
Aerospace Sciences Meeting and Exhibit
Reno, NV
January 11-14, 1999

October 23, 1998

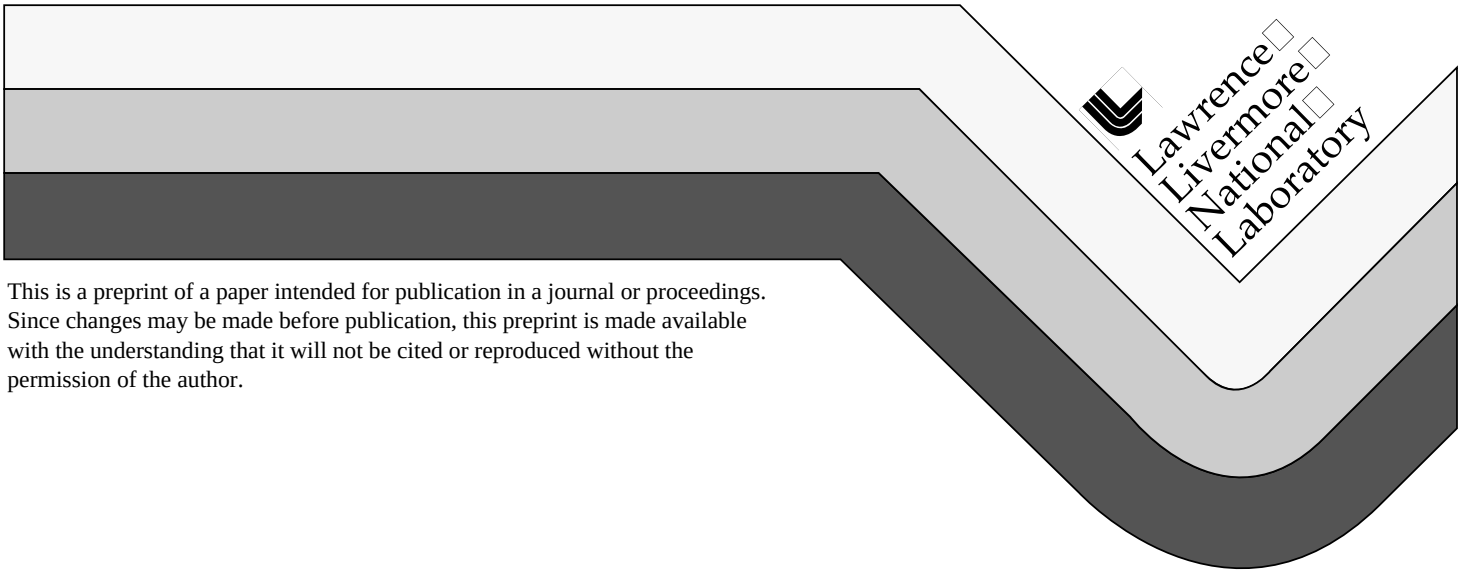

High Accuracy Capture of Curved Shock Fronts Using the Method of Space-Time Conservation Element and Solution Element

Grant Cook, Jr.
Lawrence Livermore National Laboratory
October 23, 1998

AIAA-99-1008

HIGH ACCURACY CAPTURE OF CURVED SHOCK FRONTS USING THE METHOD OF SPACE-TIME CONSERVATION ELEMENT AND SOLUTION ELEMENT

Grant Cook, Jr.
Lawrence Livermore National Laboratory
Livermore, California

Abstract

Split numerical methods have been commonly used in computational physics for many years due to their speed, simplicity, and the accessibility of shock capturing methods in one-dimension. For a variety of reasons, it has been challenging to determine just how accurate operator split methods are, especially in the presence of curved wave features. One of these difficulties has been the lack of multidimensional shock capturing methods. Another is the difficulty of mathematical analysis of discontinuous flow phenomena. Also, computational studies have been limited due to a lack of multidimensional model problems with analytic solutions that probe the nonlinear features of the flow equations. However, a new genuinely unsplit numerical method has been invented. With the advent of the Space-Time Conservation Element/Solution Element (CE/SE) method, it has become possible to attain high accuracy in multidimensional flows, even in the presence of curved shocks. Examples presented here provide some new evidence of the errors committed in the use of operator split techniques, even those employing "unsplit" corrections. In these problems, the CE/SE method is able to maintain the original cylindrical symmetry of the problem and track the main features of the flow, while the operator split methods fail to maintain symmetry and position the shocks incorrectly, particularly near the focal point of the incoming waves.

Introduction

Numerous attempts have been made over the long history of CFD to overcome grid-alignment features of the techniques for simulating shock and flow phenomena. This multidimensional simulation issue has been rendered more difficult by the use of one-dimensional splitting approaches to solving multidimensional flow equations such as the Euler equations. In addition to grid-alignment problems in flow simulation, other serious issues in multidimensional flow include accurately reproducing the curvature of shocks in the flow and minimizing reflections of waves exiting the computational domain obliquely at an absorbing boundary. In this paper, the focus will be on the issue of propagating curved shocks.

Multidimensional upwind schemes and unsplit adjustments to dimensionally split shock capturing methods such as most Godunov-based approaches have had some success in dealing with grid-alignment issues.[6, 7, 9] With some one-dimensional shock-capturing methods, it has been argued that it is possible to perform fixups to the transverse component of the flow by estimating the error incurred with the operator splitting.[5, 7] However, they have only moderate success in accurately representing curved shocks. Here, we intend to illustrate the magnitude of this problem, and to visibly demonstrate that at least one unique method does not suffer this deficiency. This method is the Space-Time Conservation Element and Solution Element (CE/SE) method due to Chang.[1] Among its many strengths is that it is genuinely unsplit from the start. It is highly accurate in 2D and 3D, as well as 1D.

In addition to the CE/SE method there is at least one other means to obtain genuinely unsplit methods. It is the Riemann Invariant Manifold theory[8] which can be used with a variety of one-dimensional methods. This approach will not be considered further here.

Some of the unique aspects of the CE/SE method are: first, it is genuinely unsplit (directionally unsplit); sec-

ond, it conserves space-time flux both locally and globally; third, neither interpolation nor extrapolation is required for flux evaluation; and fourth, through the addition of an adjustable dissipation, the method becomes robust for strong shocks. Notably, shock capture is achieved without a characteristic decomposition or the need to solve a Riemann problem.

In the next section, we sketch the essentials of the CE/SE method, including the generalization of Chang's flux limiter[2] to a 2D rectangular grid. Following that, some details are given of how the CE/SE method is applied to the two-dimensional Euler equations. Two test problems representing convergent and divergent 2D shocks are then described, the results obtained for these problems with the CE/SE method and two variants of dimensionally-split Godunov are compared. Finally, we conclude by noting where these results will be important.

The CE/SE Method

Chang and his coworkers have shown that the propagation of signals in hyperbolic conservation laws implies that it is beneficial to formulate the solution process as a leapfrog method.[1] It is easy to select conservation elements to allow a leapfrog update. Each conservation element (CE) is a region in space-time over which the integral form of each conservation law is valid. Conservation elements are chosen to fill in the space-time problem domain. While many choices are possible, we choose rectangular brick volumes in space-time for the conservation elements in the simulation code used here.

Next, the solution elements (SE) are selected as the domains over which values of the dependent variables are needed in integrals arising from the integral form of the conservation laws. In these domains a convenient representation for the dependent variables is selected. Usually, this is a Taylor series representation that is expanded about a center point in the solution element. For instance, in two dimensions on a rectangular grid that lines up with the coordinate axes, we pick the following representation for a dependent variable g.

$$g(x, y, t, x_i, y_j, t^n) = g^n_{i,j} + \left(\frac{\partial g}{\partial t}\right)^n_{i,j}(t - t^n) \quad (1)$$

$$+ \left(\frac{\partial g}{\partial x}\right)^n_{i,j}(x - x_i) + \left(\frac{\partial g}{\partial y}\right)^n_{i,j}(y - y_j)$$

$$+ \left(\frac{\partial^2 g}{\partial x \partial y}\right)^n_{i,j}(x - x_i)(y - y_j)$$

Note that 'n' denotes a time level, 'i' denotes an index in the x direction, and 'j' an index in the y direction. These indices specify the center point of the solution element that is the domain of validity for equation 1.

As shown in Figure 1, typically two solution elements are involved in the integration of a conservation law over a CE. The expansion points for the Taylor series in each solution element are denoted by the bullet symbol. One of these solution elements involves known quantities from the past time level. The other solution element is that for the unknown advanced-time values of the coefficients in the corresponding Taylor series.

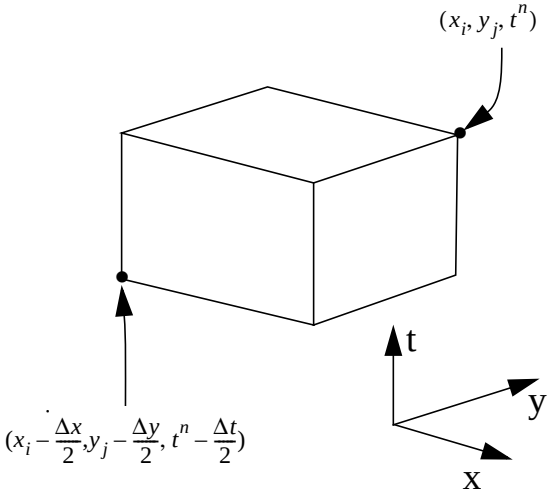

Figure 1. A typical conservation element with two Taylor series expansion points associated with solution elements that cover the surfaces and volume of the conservation element.

In the Taylor series expansion, $\left(\frac{\partial g}{\partial t}\right)^n_{i,j}$ is determined from the partial differential equation for g. The remaining four unknowns, $g^n_{i,j}$, $\left(\frac{\partial g}{\partial x}\right)^n_{i,j}$, $\left(\frac{\partial g}{\partial y}\right)^n_{i,j}$, and $\left(\frac{\partial^2 g}{\partial x \partial y}\right)^n_{i,j}$ are found by solving the four equations obtained by integrating the conservation law for g over the four individual conservation elements surrounding the update point (x_i, y_j, t^n). Figure 2 shows the four conservation elements that surround a given update point in a uniform rectangular Cartesian coordinate system. The CE labelled I is the same CE illustrated in Figure 1. This sketch also makes it a little clearer how one leapfrog time step works. It also motivates the fact that when the

integrals for two adjacent CEs are added together, the contribution on the common face is zero.

Note that no dissipation is involved in obtaining these coefficients in the Taylor series. Of course, in order to prevent ringing at shock fronts, dissipation must be added to the non-dissipative solution. Originally, Chang used a two parameter dissipation model for damping this ringing. By treating the CE of dissipation model as the union of the CEs surrounding an update point (x_i, y_j, t^n), a method for conservatively modifying the derivative coefficients was obtained. Recently, Chang refined this technique with a three parameter dissipation model.[3]

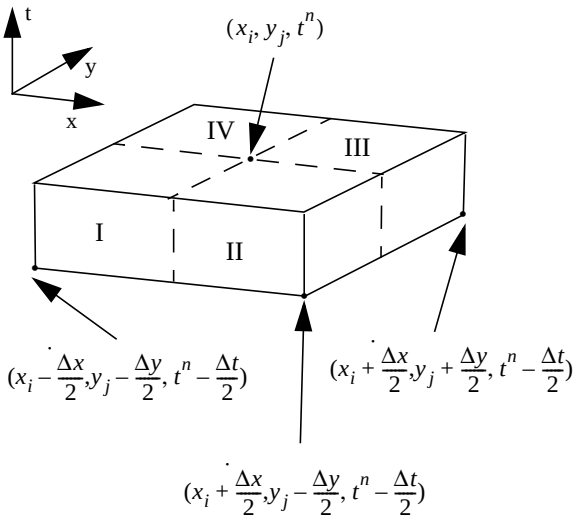

Figure 2. A typical arrangement of conservation elements surrounding an update point in leapfrog position. The solution element Taylor series expansion point at the old time level (n-1/2) for CE IV is not visible.

The basic idea behind this new dissipation model is to separately damp weak waves and strong shocks. This is indicated in equation 2, where ε is the parameter for damping weak waves and β is the parameter for damping shocks.

$$g_x^{\text{diss}} = g_x^{\text{non-diss}} + 2\varepsilon(g_x^c - g_x^{\text{non-diss}}) + \beta(g_x^w - g_x^c), \qquad (2)$$

where g_x^c is a central difference approximation to g_x, g_x^w is a nonlinear weighted average of one-sided approximations to g_x, and

$$g_x^{\text{non-diss}} = \left.\frac{\partial g}{\partial x}\right|_{CE}, \qquad (3)$$

is the solution obtained for $\left(\frac{\partial g}{\partial x}\right)_{i,j}^n$ when solving the four equations obtained from integrating over the CEs I, II, III, and IV in Figure 2.

In order to compute g_x^c and g_x^w, it is first necessary to obtain some advanced-time estimates from the previous time level data. To accomplish this, the Taylor series is used:

$$g^n_{i\pm\frac{1}{2},\, j\pm\frac{1}{2}} \approx g^{\,n-\frac{1}{2}}_{i\pm\frac{1}{2},\, j\pm\frac{1}{2}} + \frac{\Delta t}{2}\left(\frac{\partial g}{\partial t}\right)^{n-\frac{1}{2}}_{i\pm\frac{1}{2},\, j\pm\frac{1}{2}}. \qquad (4)$$

g_x^c is found from these values as follows:

$$g_x^c = \frac{\left(g^n_{i+\frac{1}{2},\, j+\frac{1}{2}} + g^n_{i+\frac{1}{2},\, j-\frac{1}{2}}\right) - \left(g^n_{i-\frac{1}{2},\, j+\frac{1}{2}} + g^n_{i-\frac{1}{2},\, j-\frac{1}{2}}\right)}{2\Delta x} \qquad (5)$$

Coupling $g^n_{i\pm\frac{1}{2},\, j\pm\frac{1}{2}}$ with the known value at the update point, $g^n_{i,j}$, four planes can be constructed, one in each of the $\pm x$ and $\pm y$ directions. For the i$^{\text{th}}$ such plane, the x and y derivatives of g can be computed. Then, if $g_x^{(i)}$ and $g_y^{(i)}$ are the derivatives on the i$^{\text{th}}$ plane, define

$$\theta_i = \sqrt{\left(g_x^{(i)}\right)^2 + \left(g_y^{(i)}\right)^2}. \qquad (6)$$

With this quantity, the nonlinear weighted average of g_x can be defined as:

$$g_x^w = [(\theta_2\theta_3\theta_4)^\alpha g_x^{(1)} + (\theta_1\theta_3\theta_4)^\alpha g_x^{(2)} + (\theta_1\theta_2\theta_4)^\alpha g_x^{(3)} + (\theta_1\theta_2\theta_3)^\alpha g_x^{(4)}]/[(\theta_2\theta_3\theta_4)^\alpha + (\theta_1\theta_3\theta_4)^\alpha + (\theta_1\theta_2\theta_4)^\alpha + (\theta_1\theta_2\theta_3)^\alpha] \qquad (7)$$

with α usually chosen to be 1.0 or 2.0. g_y^w is computed analogously. This limiter is the generalization for a rectangular grid of Chang's two-dimensional limiter on a regular triangular grid.[2]

It is also important to note that g_x^w is computed in a way that introduces no directional bias. This generalized multidimensional limiter preserves the genuinely unsplit nature of the CE/SE method. Thus, unlike techniques based upon Godunov or Riemann solvers, there are no

fixups or adjustments required to accommodate coupling between different directions.

It is most common to use an artificial viscosity as a way of adding dissipation to a physical model. Since an artificial viscosity is added to the physical pressure, it is therefore the case that linear changes in the artificial viscosity introduce nonlinear changes in the solution. By contrast, the CE/SE dissipation model introduces changes in the derivative coefficients that are linear in the amount of dissipation added. Furthermore, the dissipation is added only after the non-dissipative solution is computed. Chang found that the addition of this dissipation breaks the space-time invariance properties that a non-dissipative CE/SE method possesses.[1]

The overall result is that the CE/SE model provides better control of the dissipation than methods that introduce dissipation inside of a nonlinear operator. The CE/SE dissipation model also yields more readily to mathematical analysis.

Applying CE/SE to the 2D Euler Equations

For the two dimensional Euler equations in Cartesian coordinates, we solve the equations in internal energy form. That is, the dependent variables are chosen to be $(\rho, \rho v_x, \rho v_y, e_{\text{int}})$. We choose to denote the x and y components of the momentum by p_x and p_y; that is, $p_x = \rho v_x$ and $p_y = \rho v_y$ respectively. Also, the symbol P denotes the pressure, and should not be confused with the momentum components.

We illustrate the application of the CE/SE method to this situation by examining the conservation law for p_y. The first step is to write the integral form of the conservation law for p_y beginning with equation 8:

$$\int_{x_i}^{x_i+\frac{\Delta x}{2}}\int_{y_j}^{y_j+\frac{\Delta y}{2}}\int_{t^n-\frac{\Delta t}{2}}^{t^n}\left(\frac{\partial p_y}{\partial t} + \frac{\partial}{\partial x}\left(\frac{p_x p_y}{\rho}\right) + \frac{\partial}{\partial y}\left(P + \frac{p_x^2}{\rho}\right)\right)dx\,dy\,dt = 0 \tag{8}$$

Because of the use of conservation form, the three terms can be integrated once as shown in expressions 9, 10, and 11. Note that the term in each equation that is not at the update point uses old time level data (at $t = t^n - \frac{\Delta t}{2}$).

$$\int_{x_i}^{x_i+\frac{\Delta x}{2}}\int_{y_j}^{y_j+\frac{\Delta y}{2}}((p_y)^n - (p_y)^{n-1/2})dx\,dy \tag{9}$$

$$\int_{y_j}^{y_j+\frac{\Delta y}{2}}\int_{t^n-\frac{\Delta t}{2}}^{t^n}\left(\left(\frac{p_x p_y}{\rho}\right)\Big|_{i+1/2} - \left(\frac{p_x p_y}{\rho}\right)\Big|_{i}\right)dy\,dt \tag{10}$$

$$\int_{x_i}^{x_i+\frac{\Delta x}{2}}\int_{t^n-\frac{\Delta t}{2}}^{t^n}\left(\left(P + \frac{p_x^2}{\rho}\right)\Big|_{j+1/2} - \left(P + \frac{p_x^2}{\rho}\right)\Big|_{j}\right)dx\,dt \tag{11}$$

Now define the two flux terms in equation 8 as:

$$F^n_{i,j} = \frac{(p_x)^n_{i,j}(p_y)^n_{i,j}}{\rho^n_{i,j}} \qquad G^n_{i,j} = P^n_{i,j} + \frac{(p_x^2)^n_{i,j}}{\rho^n_{i,j}} \tag{12}$$

The Taylor series for p_y can be used to evaluate the integrals in expression 9. In order to obtain comparable results in the integrals in expressions 10 and 11, one choice is to linearize the flux terms as in equations 13 and 14.

$$F(y,t,i,j,n) = F^n_{i,j} + \left(\frac{\partial F}{\partial t}\right)^n_{i,j}(t-t^n) + \left(\frac{\partial F}{\partial y}\right)^n_{i,j}(y-y_j) \tag{13}$$

$$G(x,t,i,j,n) = G^n_{i,j} + \left(\frac{\partial G}{\partial t}\right)^n_{i,j}(t-t^n) + \left(\frac{\partial G}{\partial x}\right)^n_{i,j}(x-x_i) \tag{14}$$

In evaluating $\frac{\partial F}{\partial t}$ and $\frac{\partial G}{\partial t}$, the time derivatives of the dependent variables are encountered. Just as $\left(\frac{\partial p_y}{\partial t}\right)^n_{i,j}$ in the Taylor series for p_y is replaced by its value from the differential equation that defines it, each time derivative in $\frac{\partial F}{\partial t}$ and $\frac{\partial G}{\partial t}$ is replaced by the corresponding differential equation definition. This process is repeated for the conservation integrals over CE_I, CE_{II}, and CE_{IV}. Thereby, we obtain four equations to solve for $(p_y)^n_{i,j}$, $\left(\frac{\partial p_y}{\partial x}\right)^n_{i,j}$, $\left(\frac{\partial p_y}{\partial y}\right)^n_{i,j}$, and $\left(\frac{\partial^2 p_y}{\partial x \partial y}\right)^n_{i,j}$. Because the grid is uniform in this case, if the results of integrating over the four CEs are added together, we obtain an expression that depends only upon p_y, and not any of its derivatives. Consequently, the dependent variables can be partially updated on this grid without the need for solving a system of equations. When $\varepsilon = \frac{1}{2}$, it is not necessary to solve for the non-dissipative derivative coefficients. However, this is a large amount of dissipation; so, for

higher accuracy, it is recommended to solve three of the p_y equations for the derivative coefficients. When integrating internal energy equation over a CE, nonlinear terms are found due to the cross derivatives of kinetic energy terms. Hence, in this case, a nonlinear solver is required to solve the full system of equations. Happily, the nonlinearity is weak, so functional iteration works well given a good starting guess.

It is of interest to compare actual implementations of the CE/SE method and a Godunov method. Our CE/SE implementation on rectangular grids with $\varepsilon = \frac{1}{2}$ and $\beta = 1$ is faster per major time step (two leapfrog steps in a major time step) than the Godunov solver. Also, we observed that the CE/SE implementation is able to get reliable solutions at larger time steps than the Godunov method. These observations have been made in a framework where both the CE/SE method and a Godunov method are implemented in the same simulation code, and in a way so that both use exactly the same underlying simulation code services (such as initialization, memory management, graphics, etc.). Consequently, the algorithms themselves can be directly compared for speed, accuracy, code size, etc. Since the CE/SE method involves solving for the flow variables and their gradients, it is not obvious how this can be made to be more efficient than an optimized Godunov solver. This achievement was made possible through the use of advanced symbolic computing tools for the bulk of the coding, very sophisticated optimization, and clever adjustments to the multidimensional limiters.

When reducing the amount of dissipation used by CE/SE, a nonlinear solver is required, and the CE/SE method then slows down to about half the speed of the Godunov solver. Considering the gains in accuracy, especially for curved features, this is an easily justified cost.

Test Problems

We illustrate curved shock issues with converging cylindrical shocks. In order to elucidate the problems that arise due to split versus unsplit methods, we pick model problems in cylindrical coordinates that depend only upon the radial coordinate. The simulation is then performed on a uniform two-dimensional rectangular Cartesian grid that lies in the (ρ,θ) cylindrical coordinate plane. The size of the grid is 128 by 128.

In the two problems considered here, the initial conditions include features that do not conform to the geometry of the grid. Hence, stairstepping errors or mesh imprinting occurs due to the initial conditions. Nonetheless, as will be seen from the CE/SE solutions, these errors are small.

The first Godunov solver used in these simulations is based upon the Direct Eulerian MUSCL scheme.[4] It employs a standard ADI-type approach for solving the multidimensional Euler equations; that is, after solving a sequence of Riemann problems in one direction, it performs transverse fixups in the directions normal to the sweep. In order to remove some bias, the order of directional sweeps is reversed from one-half time step to the next. This solver will be identified as the MUSCL solver in the following discussion.

The second Godunov solver employed is the CLAWPACK package as embedded in AMRCLAW.[7] It is a wave propagation method with an 'unsplit' character in the sense that it approximates the terms that are missing in the operator splitting of the full (nonlinear) Euler equations.

The CE/SE solver used in the simulations used the following parameter values for the dissipation model: $\varepsilon = 0.25$ and $\beta = 0.12$, with $\alpha = 1.0$ in the first problem and $\alpha = 2.0$ in the second problem. It also specified six digits of accuracy in the nonlinear solver.

All regions in these problems are made up of γ-law gases with $\gamma = \frac{5}{3}$.

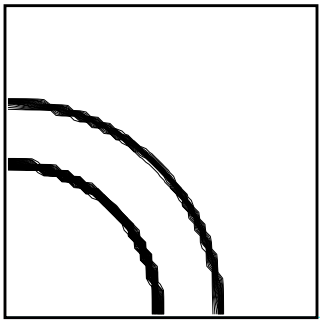

Figure 3. Initial conditions for the three region problem. The inner very low density region has a low pressure; the low density outer region has a high pressure; and the high density middle region has an intermediate pressure.

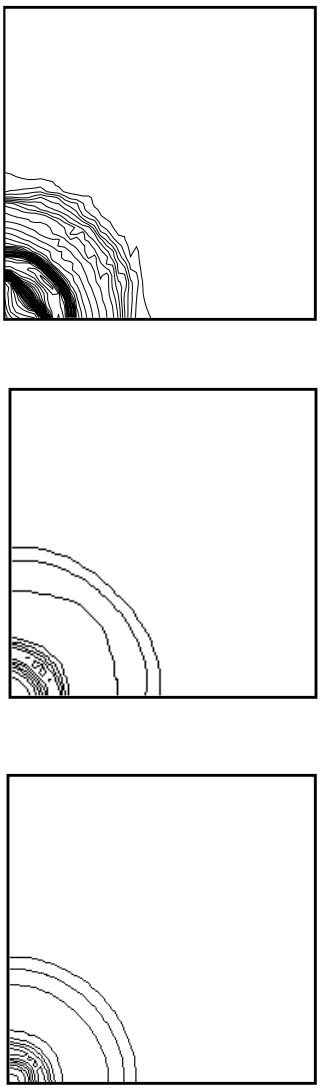

Figure 4. Problem 1 just before a major shock reaches the origin. The top plot shows the CLAWPACK result; the middle plot shows the corresponding MUSCL result; and the bottom plot shows the CE/SE result using $\alpha = 1.0$.

Figure 5. Problem 1 after the shocks have rebounded. The top plot shows the CLAWPACK result; the middle plot shows the corresponding MUSCL result; and the bottom plot shows the CE/SE result using $\alpha = 1.0$.

The first problem is a three region problem where the inner region is very low density, low pressure, the middle region is higher density and medium pressure, while the outer region is low density and high pressure. Each region is bounded by cylindrical surfaces. The initial density contours are shown in Figure 3.

Note from the Godunov solutions in Figure 4 that just before the main shock reaches the lower left corner of the plot, the MUSCL result is showing subtle hints of flattening in the solution along the diagonal of the grid (where *x=y, x* and *y* being the two Cartesian coordinates)). In the CLAWPACK solution, the flattening is very pronounced. A short while after the main shock bounce is seen in Figure 5. A significant deterioration of both Godunov solutions near the origin has clearly occurred. In fact, in addition to flattening of the shocks, there appears to be jetting occurring on the coordinate

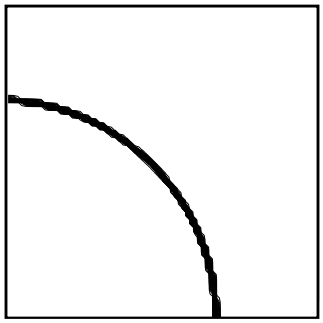

Figure 6. Initial conditions for the two region problem. The inner low density region has a low pressure, and the medium density outer region has an intermediate pressure.

axes near the origin. In the CE/SE solution, there is slight squaring of the contours out a short distance from the origin. Also, a minor manifestation of the mesh imprinting of the initial conditions is visible. But overall, the CE/SE solution is excellent.

The second problem is a two region problem where the inner region is a low density, low pressure gas, and the outer region is a medium density and medium pressure gas. Once again, the regions are bounded by a cylindrical surface.Contours of this setup are shown in Figure 6.

From Figure 7, just before the main shock reaches the lower left corner of the plot, slight hints of flattening appear in the Godunov solutions along the diagonal of the grid occurs. The effect is not as strong as in the first problem. However, color contour plots definitely reveal the effect. For the CE/SE method, mesh imprinting may have caused one contour to be slightly flattened. In this case, color contour plots only show a slight asymmetry in the solution.

A short while after the main shock bounce, the Godunov solutions in Figure 8 both show significant deterioration near the origin. In this case, jetting occurs on the coordinate axes near the origin, although not as pronounced as in the three region problem. As before, the CE/SE solution appears to be cylindrically symmetric.

These results establish beyond a doubt that the genuinely unsplit CE/SE technique is quite powerful. Using a square Cartesian grid, curved shocks are propagated almost without distortion across a grid that at no point in

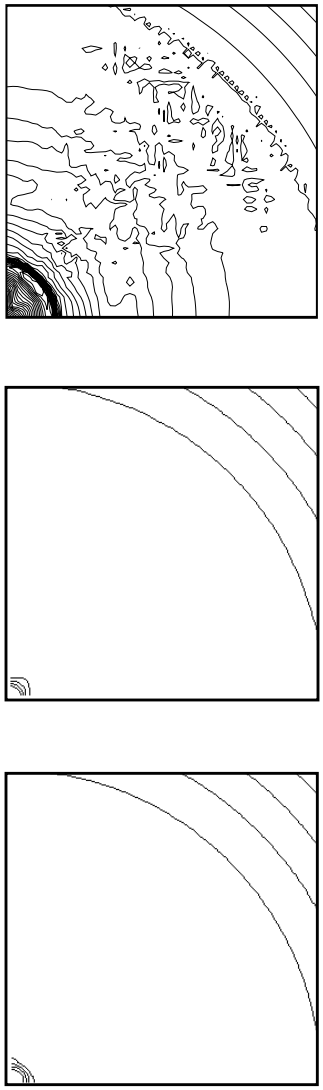

Figure 7. Problem 2 just before the main shock reaches the origin. The top plot shows the CLAWPACK result; the middle plot shows the corresponding MUSCL result; and the bottom plot shows the CE/SE result using $\alpha = 2.0$.

the simulation matches the shape of the shocks. It is also clear that very serious errors can arise due to the use of dimensional splitting in solvers of nonlinear equations. From our experience, the evidence points to the dimensional splitting errors becoming visible when the curvature of a shock becomes large in a single zone of the grid.

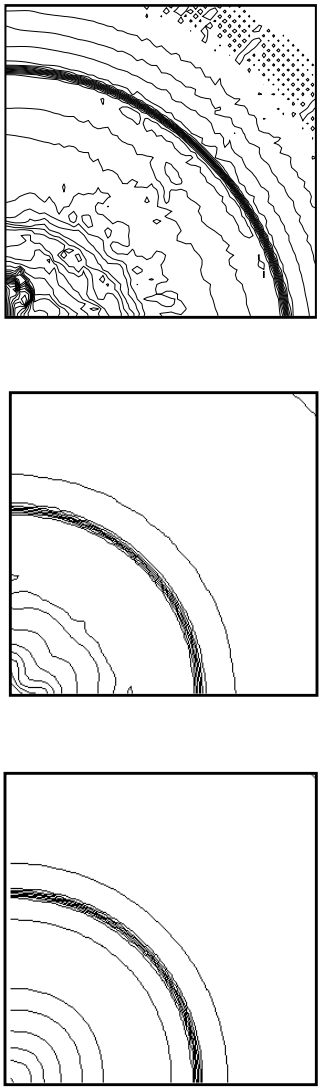

Figure 8. Problem 2 after the shock has rebounded. The top plot shows the CLAWPACK result; the middle plot shows the corresponding MUSCL result; and the bottom plot shows the CE/SE result using $\alpha = 2.0$.

Conclusions

The ramifications of these results are not limited to the case when a shock has curvature. Any nonuniform flow, particularly one developing instabilities or turbulence, will be more faithfully simulated by a technique like the CE/SE method. This method's genuinely unsplit character is critical to its accuracy in the tests presented here and points clearly to its potential in more demanding flow problems.

Acknowledgments

This work was performed under the auspices of the U. S. Department of Energy by the Lawrence Livermore National Laboratory, under contract number W-7405-ENG-48.

References

[1] S. C. Chang, "The Method of Space-Time Conservation Element and Solution Element - A New Approach for Solving the Navier-Stokes and Euler Equations," *J. Comput. Phys.* **119**, 295 (1995).

[2] S. C. Chang, X. Y. Wang, and C. Y. Chow, "The Method of Space-Time Conservation Element and Solution Element - Applications to One-Dimensional and Two-Dimensional Time-Marching Flow Problems," AIAA paper 95-1754, presented at the 12th AIAA Computational Fluid Dynamics Conference, San Diego, California, June 19-22, 1995.

[3] S. C. Chang, X. Y. Wang, and C. Y. Chow, "The Space-Time Conservation Element and Solution Element Method - A New High-Resolution and Genuinely Multidimensional Paradigm for Solving Conservation Laws I. The Two-Dimensional Time Marching Schemes," 1998, submitted.

[4] Phillip Colella, "A Direct Eulerian MUSCL Scheme for Gas Dynamics", *SIAM J. Sci. Comput.* **6** (1), 104 (1985).

[5] W. Dai and P. R. Woodward, "A Second-Order Unsplit Godunov Scheme for Two- and Three-Dimensional Euler Equations," *J. Comput. Phys.* **134**, 261 (1997).

[6] L. A. Khan and P. L.-F. Liu, "Numerical analyses of operator-splitting algorithms for the two-dimensional advection-diffusion equation," *Comput. Methods Appl. Mech. Engrg*. **152**, 337 (1998).

[7] R. J. LeVeque, "Wave Propagation Algorithms for Multidimensional Hyperbolic Systems," *J. Comput. Phys.* **131**, 327 (1997).

[8] M. V. Papalexandris, A. Leonard, P. E. Dimotakis, "Unsplit Schemes for Hyperbolic Conservation-Laws with Source Terms in One Space Dimension," *J. Comput. Phys.* **134**, 31 (1997).

[9] J. Saltzman, "An Unsplit 3D Upwind Method for Hyperbolic Conservation Laws," *J. Comput. Phys.* **115**, 153 (1994).